First measurement of differential cross sections for muon neutrino charged current interactions on argon with a two-proton final state using the MicroBooNE detector

P. Abratenko[an], O. Alterkait[an], D. Andrade Aldana[o], L. Arellano[v], J. Asaadi[am], A. Ashkenazi[ak], S. Balasubramanian[l], B. Baller[l], A. Barnard[ac], G. Barr[ac], D. Barrow[ac], J. Barrow[z], V. Basque[l], J. Bateman[p,v], L. Bathe-Peters[n], O. Benevides Rodrigues[o], S. Berkman[y], A. Bhanderi[v], A. Bhat[g], M. Bhattacharya[l], M. Bishai[c], A. Blake[s], B. Bogart[x], T. Bolton[r], J. Y. Book[n], M. B. Brunetti[ap], L. Camilleri[j], Y. Cao[v], D. Caratelli[d], I. Caro Terrazas[i], F. Cavanna[l], G. Cerati[l], A. Chappell[ap], Y. Chen[ag], J. M. Conrad[w], M. Convery[ag], L. Cooper-Troendle[ad], J. I. Crespo-Anadón[f], R. Cross[ap], M. Del Tutto[l], S. R. Dennis[e], P. Detje[e], A. Devitt[s], R. Diurba[b], Z. Djurcic[a], R. Dorrill[o], K. Duffy[ac], S. Dytman[ad], B. Eberly[ai], P. Englezos[af], A. Ereditato[g,l], J. J. Evans[v], C. Fang[d], O. G. Finnerud[v], R. Fine[t], B. T. Fleming[g], W. Foreman[o,t], N. Foppiani[n], D. Franco[g], A. P. Furmanski[z], F. Gao[d], D. Garcia-Gamez[m], S. Gardiner[l], G. Ge[j], S. Gollapinni[t], E. Gramellini[v], P. Green[ac], H. Greenlee[l], L. Gu[s], W. Gu[c], R. Guenette[v], P. Guzowski[v], L. Hagaman[g], M. D. Handley[e], O. Hen[w], R. Hicks[t], C. Hilgenberg[z], G. A. Horton-Smith[r], A. Hussain[r], Z. Imani[an], B. Irwin[x], M. S. Ismail[ad], R. Itay[ag], C. James[l], X. Ji[aa], L. Jiang[ao], J. H. Jo[c], R. A. Johnson[h], Y.-J. Jwa[j], D. Kalra[j], N. Kamp[w], G. Karagiorgi[j], W. Ketchum[l], M. Kirby[c], T. Kobilarcik[l], I. Kreslo[b], N. Lane[p,v], I. Lepetic[af], J.-Y. Li[k], K. Li[aq], Y. Li[c], K. Lin[af], H. Liu[c], B. R. Littlejohn[o], L. Liu[l], W. C. Louis[t], X. Luo[d], T. Mahmud[s], C. Mariani[ao], D. Marsden[v], J. Marshall[ap], N. Martinez[r], D. A. Martinez Caicedo[ah], S. Martynenko[c], A. Mastbaum[af], I. Mawby[s], N. McConkey[ae], V. Meddage[r], L. Mellet[y], J. Mendez[u], J. Micallef[w,an], K. Miller[g], A. Mogan[i], T. Mohayai[q], M. Mooney[i], A. F. Moor[e], C. D. Moore[l], L. Mora Lepin[v], M. M. Moudgalya[v], S. Mulleriababu[b], D. Naples[ad], A. Navrer-Agasson[p,v], N. Nayak[c], M. Nebot-Guinot[k], C. Nguyen[af], J. Nowak[s], N. Oza[j], O. Palamara[l], N. Pallat[z], V. Paolone[ad], A. Papadopoulou[a], V. Papavassiliou[ab], H. B. Parkinson[k], S. F. Pate[ab], N. Patel[s], Z. Pavlovic[l], E. Piasetzky[ak], K. Pletcher[y], I. D. Ponce-Pinto[aq], I. Pophale[s], S. Prince[n], X. Qian[c], J. L. Raaf[l], V. Radeka[c], A. Rafique[a], M. Reggiani-Guzzo[k], L. Ren[ab], J. Rodriguez Rondon[ah], M. Rosenberg[an], M. Ross-Lonergan[t], C. Rudolf von Rohr[b], I. Safa[j], G. Scanavini[aq], D. W. Schmitz[g], A. Schukraft[l], W. Seligman[j], M. H. Shaevitz[j], R. Sharankova[l], J. Shi[e], E. L. Snider[l], M. Soderberg[aj], S. Söldner-Rembold[p,v], J. Spitz[x], M. Stancari[l], J. St. John[l], T. Strauss[l], S. Sword-Fehlberg[ab], A. M. Szelc[k], W. Tang[al], N. Taniuchi[e], K. Terao[ag], C. Thorpe[v], D. Torbunov[c], D. Totani[d], M. Toups[l], A. Trettin[v], Y.-T. Tsai[ag], J. Tyler[r], M. A. Uchida[e], T. Usher[ag], B. Viren[c], J. Wang[aa], M. Weber[b], H. Wei[u], A. J. White[g], S. Wolbers[l], T. Wongjirad[an], M. Wospakrik[l], K. Wresilo[e], W. Wu[ad], E. Yandel[d,t], T. Yang[l], L. E. Yates[l], H. W. Yu[c], G. P. Zeller[l], J. Zennamo[l], C. Zhang[c],

(The MicroBooNE Collaboration)*

[a]*Argonne National Laboratory (ANL), Lemont, IL, 60439, USA*
[b]*Universität Bern, Bern CH-3012, Switzerland*
[c]*Brookhaven National Laboratory (BNL), Upton, NY, 11973, USA*
[d]*University of California, Santa Barbara, CA, 93106, USA*
[e]*University of Cambridge, Cambridge CB3 0HE, United Kingdom*
[f]*Centro de Investigaciones Energéticas, Medioambientales y Tecnológicas (CIEMAT), Madrid E-28040, Spain*
[g]*University of Chicago, Chicago, IL, 60637, USA*
[h]*University of Cincinnati, Cincinnati, OH, 45221, USA*
[i]*Colorado State University, Fort Collins, CO, 80523, USA*

*j*Columbia University, New York, NY, 10027, USA

*k*University of Edinburgh, Edinburgh EH9 3FD, United Kingdom

*l*Fermi National Accelerator Laboratory (FNAL), Batavia, IL 60510, USA

*m*Universidad de Granada, E-18071, Granada, Spain

*n*Harvard University, Cambridge, MA 02138, USA

*o*Illinois Institute of Technology (IIT), Chicago, IL 60616, USA

*p*Imperial College London, London SW7 2AZ, United Kingdom

*q*Indiana University, Bloomington, IN 47405, USA

*r*Kansas State University (KSU), Manhattan, KS, 66506, USA

*s*Lancaster University, Lancaster LA1 4YW, United Kingdom

*t*Los Alamos National Laboratory (LANL), Los Alamos, NM, 87545, USA

*u*Louisiana State University, Baton Rouge, LA, 70803, USA

*v*The University of Manchester, Manchester M13 9PL, United Kingdom

*w*Massachusetts Institute of Technology (MIT), Cambridge, MA, 02139, USA

*x*University of Michigan, Ann Arbor, MI, 48109, USA

*y*Michigan State University, East Lansing, MI 48824, USA

*z*University of Minnesota, Minneapolis, MN, 55455, USA

*aa*Nankai University, Nankai District, Tianjin 300071, China

*ab*New Mexico State University (NMSU), Las Cruces, NM, 88003, USA

*ac*University of Oxford, Oxford OX1 3RH, United Kingdom

*ad*University of Pittsburgh, Pittsburgh, PA, 15260, USA

*ae*Queen Mary University of London, London E1 4NS, United Kingdom

*af*Rutgers University, Piscataway, NJ, 08854, USA

*ag*SLAC National Accelerator Laboratory, Menlo Park, CA, 94025, USA

*ah*South Dakota School of Mines and Technology (SDSMT), Rapid City, SD, 57701, USA

*ai*University of Southern Maine, Portland, ME, 04104, USA

*aj*Syracuse University, Syracuse, NY, 13244, USA

*ak*Tel Aviv University, Tel Aviv, Israel, 69978

*al*University of Tennessee, Knoxville, TN, 37996, USA

*am*University of Texas, Arlington, TX, 76019, USA

*an*Tufts University, Medford, MA, 02155, USA

*ao*Center for Neutrino Physics, Virginia Tech, Blacksburg, VA, 24061, USA

*ap*University of Warwick, Coventry CV4 7AL, United Kingdom

*aq*Wright Laboratory, Department of Physics, Yale University, New Haven, CT, 06520, USA

Abstract

We present the first measurement of differential cross sections for charged-current muon neutrino interactions on argon with one muon, two protons, and no pions in the final state. These final states are dominated by two-nucleon knockout interactions, which are complicated to model and for which there is currently limited information about the characteristics of these interactions in existing neutrino-nucleus scattering data. Detailed investigations of two-nucleon knockout are vital to support upcoming experiments exploring the nature of the neutrino. Among the different kinematic quantities measured, the opening angle between the two protons, the angle between the total proton momentum and the muon, and the total transverse momentum of the final state system are most sensitive to the underlying physics processes as embodied in various theoretical models.

Keywords: neutrinos, argon, cross section, charged-current interactions, 2-particle 2-hole states

*Email address: `microboone_info@fnal.gov`

1. Introduction

The introduction of the liquid argon time projection chamber (LArTPC) [1, 2, 3, 4] has revolutionized the field of accelerator-based neutrino physics, allowing more detailed observations of ionizing radiation emitted from final state particles than was previously possible. This development has highlighted the need for advanced modeling of neutrino-nucleus interactions, especially neutrino-argon interactions, and detailed measurements to benchmark those models. Cross-section measurements for various nuclei and final state topologies are needed to support the development of neutrino interaction models [5]. These models must address both in-medium nuclear modification of the fundamental neutrino interactions and also final-state interactions (FSI) involving the reaction products as they exit the nucleus [6].

One process that probes both neutrino interactions and nuclear effects is the production of two-particle two-hole (2p2h) states in which two nucleons are removed from the nucleus. These states are primarily produced by neutrino interactions where the momentum transfer is shared between two nucleons via the exchange of a virtual meson, known as a meson exchange current (MEC) [6]. In addition, 2p2h states can be produced by nuclear effects, such as short-range nucleon-nucleon correlations (SRC) [7, 8] and FSI. In the case of SRCs, the neutrino interacts with a nucleon that is part of a correlated nucleon-nucleon pair. The momentum is transferred to a single nucleon but, because this nucleon is part of a correlated pair, both nucleons are knocked out of the nucleus. In the case of FSI, it is possible for a single nucleon to knock out a second nucleon as it exits the nucleus thereby leading to a 2p2h final state. Observation of 2p2h states in electron scattering has been used to develop the models of 2p2h production in neutrino scattering [9, 10]. Correct modeling of 2p2h interactions is of vital importance to neutrino energy reconstruction and precision measurements of neutrino oscillations. Difficulty in measuring this production mode has required large variations to models to agree with data [11, 12] and has the potential to bias energy reconstruction if the prediction of the 2p2h production cross section is incorrect [13, 14].

A final state topology consistent with the production of a 2p2h state is a charged-current (CC) muon neutrino (ν_μ) interaction that results in one muon, two protons, and no charged or neutral pions (CC1μ2p0π). While there is an existing measurement of CC1μ2p0π events on argon, no cross sections were extracted [15]. In this letter, we present the first differential cross section measurements of CC1μ2p0π topologies on argon using data collected from the Micro Booster Neutrino Experiment (MicroBooNE) [16].

2. Detector and Samples

The MicroBooNE experiment uses an 85 metric ton active volume LArTPC detector located at Fermi National Accelerator Laboratory [16]. The detector is situated on-axis to the Booster Neutrino Beam (BNB) which has an average energy of $\langle E_\nu \rangle = 0.8$ GeV [17] and is located approximately 470 m from the neutrino production target. The detector consists of two components: a TPC, 10.36 m long in the beam direction, 2.56 m wide in the drift direction, and 2.32 m tall; and an optical system comprised of 32 eight-inch photomultiplier tubes (PMTs). The TPC consists of three wire planes, two induction planes and one collection plane. The collection plane is oriented vertically and the induction plane wires are oriented at angles ±60° with respect to the vertical direction. Electronic signals from the TPC wire planes and the PMTs are recorded and subdivided into two distinct data samples. The first sample, known as on-beam data (BNB data), is collected coincident to a 1.6 μs BNB neutrino spill. The second sample, known as off-beam

data (EXT data), is recorded in anti-coincidence with the beam. This sample provides a measure of the electronic noise and large cosmic muon background caused by the surface location of the MicroBooNE detector. The BNB data and a portion of the EXT data samples are then filtered based on a required minimum amount of activity measured in the PMTs. This study uses data from the three-year period 2016-2018, corresponding to 6.85×10^{20} protons on target.

MicroBooNE utilizes the GENIE neutrino event generator [18] to create two samples of simulated neutrino interactions: Monte Carlo which addresses signal events and beam-related backgrounds (Beam MC), and Monte Carlo which addresses backgrounds from neutrino interactions in the material surrounding the cryostat (Dirt MC). The simulated events from both samples are then combined with events from an unbiased EXT sample (which is not filtered based on PMT activity) in order to simulate MicroBooNE's cosmic ray background [19]. Furthermore, Micro-BooNE utilizes another sample of simulated events generated using the NuWro neutrino event generator [20] for additional studies.

The neutrino-argon scattering model in both the Beam MC and Dirt MC samples is given by the GENIE MicroBooNE Tune, a version of the GENIE v3.0.6 G18_10a_02_11a model set in which four parameters are tuned to ν_μ CC0π data from the T2K experiment [12]. The four parameters are: the CC quasi-elastic axial mass [21], the strength of the random phase approximation (RPA) corrections in the Nieves CCQE cross section calculation [22], the absolute normalization of the CC2p2h cross section [23], and the shape of the CC2p2h cross-section. The shape of the CC2p2h cross section is represented by a parameter that linearly interpolates between two models: the Valencia prediction [23] and the Dytman model [24].

3. Event Selection

The signal consists of CC ν_μ interactions within the fiducial volume with the final state particles consisting of exactly one muon with momentum $0.1 \leq P_\mu^{\text{true}} \leq 1.2 \, \text{GeV}/c$ and two protons with momentum $0.3 \leq P_p^{\text{true}} \leq 1.0 \, \text{GeV}/c$. Events with any number of neutral pions are excluded. Signal events may also contain protons with momentum below $0.3 \, \text{GeV}/c$ or above $1.2 \, \text{GeV}/c$, any number of neutrons, and charged pions with momentum below $65 \, \text{MeV}/c$.

The BNB data, EXT data, Beam MC, and Dirt MC samples are processed by the Pandora reconstruction framework [25] to identify and reconstruct tracks from the ionized signal. The track's energy deposition and length are used to reconstruct momentum and particle identification. From the reconstructed products, a series of selection requirements are applied to identify CC1μ2p0π events. The initial selection retains events that meet three criteria: (1) the reconstructed neutrino vertex is located within a fiducial volume (FV) defined to be at least $10 \, \text{cm}$ inside any TPC face, (2) there are exactly three tracks, and no showers as determined by Pandora, (3) the three tracks start within $4 \, \text{cm}$ of the reconstructed neutrino vertex. Calorimetry-based particle identification techniques described in Ref. [26] are then used to identify events with a single muon candidate and two proton candidates.

The final event selection requires one muon with momentum in the range $0.1 \leq P_\mu^{\text{reco}} \leq 1.2 \, \text{GeV}/c$ and two protons, both with momentum in the range $0.3 \leq P_p^{\text{reco}} \leq 1.0 \, \text{GeV}/c$, to match the signal definition. The limits on momentum are driven by the resolution effects as well as phase space regions which have non-zero efficiencies and well-understood systematic uncertainties. To benchmark the performance of the selection, the number of simulated CC1μ2p0π events that pass all selection requirements is compared to the number of events generated using the GENIE MicroBooNE tune; the event selection described above achieves an efficiency and purity of $\simeq$14% and $\simeq$65%, respectively.

4

Several theoretical predictions of neutrino interactions are compared to data within this work and a detailed summary of each prediction is provided in the supplemental materials. Four GENIE model [21] sets are considered: GENIE v3.0.6 G18_02a_00_000 (GENIE Empirical), GENIE v3.0.6 G18_10a_02_11a (GENIE Nieves), GENIE v3.2.0 G21_11b_00_000 (GENIE SuSAv2), and the GENIE MicroBooNE Tune. Each of these GENIE models uses different models for QE, MEC, and FSI. The GENIE Empirical model set uses the relativistic Fermi gas (RFG) nuclear model [27], the Llewellyn Smith QE model [28], and an empirically derived prediction for MEC interactions [24]. The GENIE Nieves model set uses the local Fermi gas (LFG) nuclear model [29], which is similar to the RFG model but includes considerations for the nuclear density. The Nieves QE [30] model is similar to the Llewellyn Smith QE model, but includes contributions from long-range nucleon-nucleon correlations and Coulombic effects. The Nieves MEC model is based on a macroscopic calculation [23]. The SuSAv2 model set utilizes the relativistic mean field (RMF) approximation nuclear model [31, 32], which considers relativistic effects in the calculation of the motion of the nucleons in the nucleus. Relativistic effects are also considered in the calculation of the SuSAv2 QE [10] and SuSAv2 MEC [33] predictions by using scaling functions, derived from relativistic assumptions, to scale the cross sections at high momentum transfers. The GENIE MicroBooNE Tune is identical to the GENIE Nieves model except that two CCQE and two CC2p2h parameters are tuned to T2K data [12], as described previously.

Beyond the GENIE generator predictions, the GiBUU 2023 [34], NuWro 19.02 [35], and NEUT 5.4.0 [36] model sets are also considered. The GiBUU model set uses an LFG model [29], a standard CCQE expression [37], and an empirical MEC model. These models are consistently implemented to solve the Boltzmann-Uehling-Uhlenbeck transport equation [38]. The NuWro model set is built on the same LFG model [39], using the Llewellyn Smith QE model [28]. The FSI treatment in NuWro uses an intranuclear cascade [40] to transport the hadrons through the nucleus, along with a coupling to PYTHIA for hadronization [41]. The NEUT model set utilizes an LFG model [39], with Nieves CCQE [30] and MEC [23] scattering models, and treats FSI with medium corrections for pions [18].

Using samples of simulated ν_μ CC interactions from each model set, a study was conducted to identify variables sensitive to physics differences between the model sets. One such variable is the opening angle between the protons in the lab frame, $\theta_{\vec{P}_L \cdot \vec{P}_R}$, defined as:

$$\cos(\theta_{\vec{P}_L \cdot \vec{P}_R}) = \frac{\vec{P}_L \cdot \vec{P}_R}{\left|\vec{P}_L\right| \left|\vec{P}_R\right|} \tag{1}$$

where $\vec{P}_L$ is the momentum of the leading proton, the proton with the highest momentum, and $\vec{P}_R$ is the momentum of the recoil proton, the second proton in the event. A second physics-sensitive variable is the opening angle between the muon and total proton momentum vector, $\theta_{\vec{P}_\mu \cdot \vec{P}_{\text{sum}}}$, defined as:

$$\cos(\theta_{\vec{P}_\mu \cdot \vec{P}_{\text{sum}}}) = \frac{\vec{P}_\mu \cdot \vec{P}_{\text{sum}}}{\left|\vec{P}_\mu\right| \left|\vec{P}_{\text{sum}}\right|} \tag{2}$$

where $\vec{P}_\mu$ is the momentum of the muon and $\vec{P}_{\text{sum}}$ is the vector addition of the leading and recoil proton momenta. The opening angle between the protons in the lab frame provides information on the effect of the QE and MEC modeling on the proton momentum, while the opening angle

5

between the muon and total proton momentum vectors provides information on the treatment of the outgoing muon momentum in relation to the 2p2h system.

In addition to these two angles, we also identify the magnitude of the momentum transverse to the neutrino beam direction of the final state system, δP_T [42]. The transverse momentum vector of the CC1μ2p0π system ($\delta\vec{P}_T$) is defined as:

$$\delta\vec{P}_T = \vec{P}_T^{\mu} + \vec{P}_T^{L} + \vec{P}_T^{R} \tag{3}$$

where $\vec{P}_T^{\mu}$, $\vec{P}_T^{L}$, and $\vec{P}_T^{R}$ are the transverse momentum vectors of the muon, leading proton, and recoil proton respectively. The magnitude δP_T is sensitive to nuclear effects, final state interactions, or below threshold undetected particles.

Distributions of selected events as a function of the cosine of $\theta_{\vec{P}_L \cdot \vec{P}_R}$ can be found in Fig. 1. The colored bands in each histogram represent events selected from the MC subdivided into different final state topologies [Fig. 1(a)] and different interaction modes based on the GENIE MicroBooNE Tune prediction [Fig. 1(b)]. The error bars on the data points are the data statistical uncertainty while the dashed lines represent the uncertainty of the prediction. This uncertainty includes both the statistical uncertainty of the prediction and systematic uncertainty, which dominates over the data statistical uncertainty for this measurement. Contributions from flux modeling and protons-on-target (POT) counting [43], cross section modeling [12], re-interaction modeling [44], and detector modeling [45] are considered in the calculation of the systematic uncertainties, which was performed using the multiverse techniques described in Section V of Ref. [12]. Uncertainty on the modeling of dirt events is also considered in the systematic uncertainty [46]. We find that our CC1μ2p0π signal, represented by the blue-green bands in Fig. 1(a), constitutes the majority of the prediction. We also find that the CCMEC process, represented by the blue-green band in Fig. 1(b), has fewer events in the region of $\cos(\theta_{\vec{P}_L \cdot \vec{P}_R}) \simeq 0$ compared to the signal. This is expected as MEC is not the only contributor to CC1μ2p0π topologies.


4. Cross Section Extraction

Due to detector resolution, efficiency, and smearing effects, our reconstructed kinematic variables require unfolding to obtain the underlying physics quantities. We use the Wiener-SVD technique [47] as implemented in [48]. In this technique, any bias due to regularization introduced by the unfolding is encoded in a regularization matrix A_C which is applied to all cross-section predictions included in this work. The A_C matrix should be applied to any independent theoretical prediction compared to the data reported in this paper. The data release, unfolded covariance matrices, and A_C matrices are provided in the supplemental material.

Unfolded distributions are then normalized by the number of target nuclei and the total integrated neutrino flux to produce a cross section. We validate the Wiener-SVD unfolding technique by performing fake data studies before unfolding the selected BNB data events.

Fig. 2 shows the single differential cross sections as functions of cosine of $\theta_{\vec{P}_L \cdot \vec{P}_R}$ [Fig. 2(a)] and cosine of $\theta_{\vec{P}_\mu \cdot \vec{P}_{\text{sum}}}$ [Fig. 2(b)]. The black points represent the extracted cross section from data with the inner error bands representing the statistical uncertainty and the outer error bands representing the systematic uncertainty. The dominant uncertainties on the total event rate prediction are comprised of the systematic uncertainties on modelling MEC interactions (which enter primarily through their impact on the signal selection efficiency) and uncertainties on modelling the detector response. The fractional uncertainty in each bin ranges between 13% and 24%.
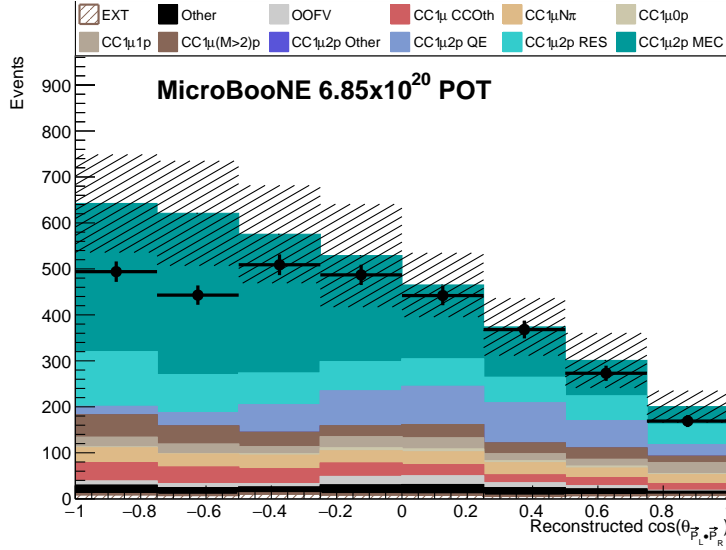
(a)
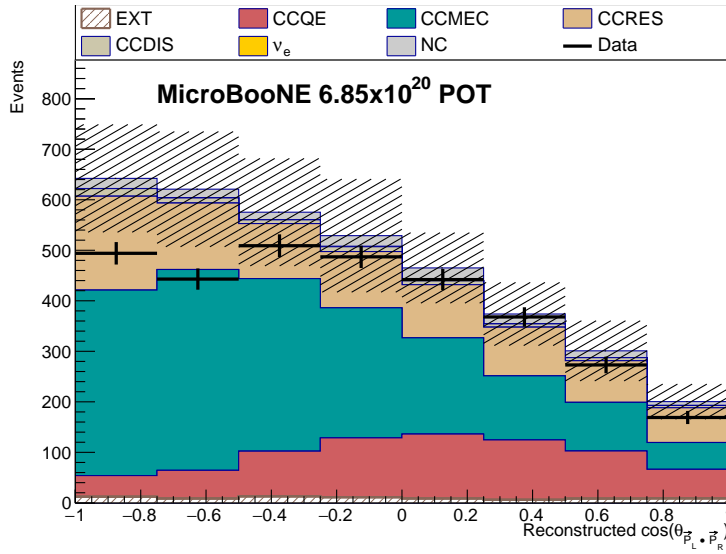
(b)

Figure 1: Yield for the cosine of the opening angle between the protons in the lab frame, $\theta_{\vec{P}_L \cdot \vec{P}_R}$. The selected MC events are broken down into (a) final-state topologies and (b) ν interaction channels based on the MicroBooNE Tune [12] truth information. The error on the data represents the data statistical uncertainty and the hatched region includes both the MC statistical uncertainty of the prediction and systematic uncertainty. Most subsamples are defined in the main text. 'OOFV' refers to interactions outside the fiducial volume. 'CC1μ(M>2)p' events are CC ν_μ interactions with more than two outgoing protons above threshold. 'CC1μOth' are any CC ν_μ interactions not included in other samples. 'Other' contains any interactions not included in another sample. 'CCRES' are resonant CC ν_μ interactions and 'CCDIS' are deep inelastic scattering CC ν_μ interactions.

7
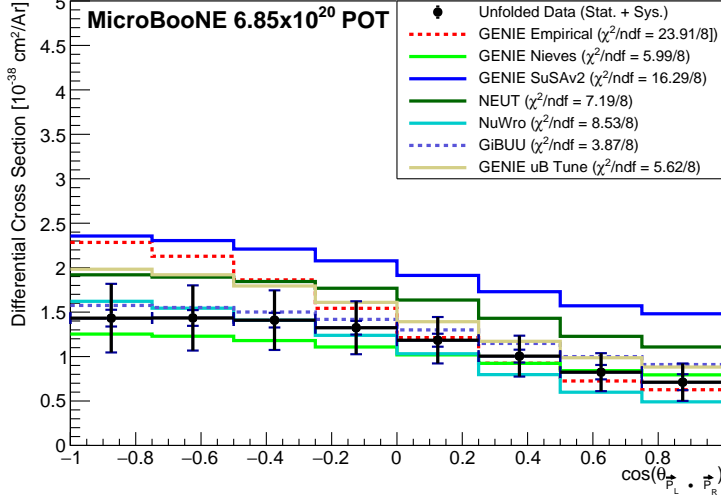
(a)
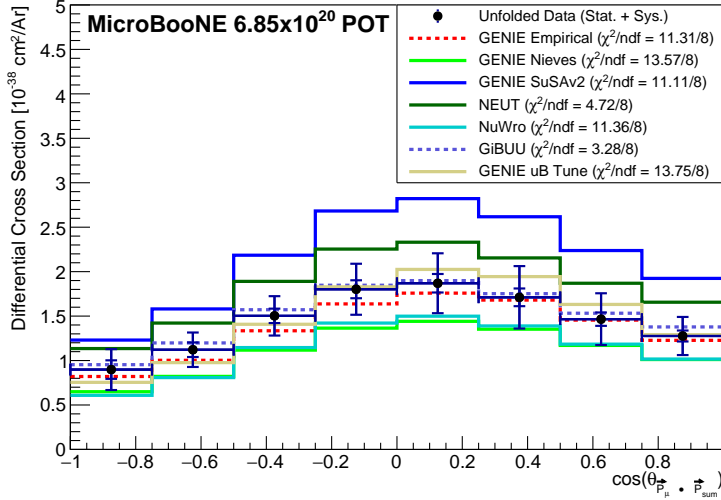
(b)

Figure 2: Single differential cross sections as a function of (a) the cosine of the opening angle between the protons in the lab frame, $\cos(\theta_{\vec{P}_L \cdot \vec{P}_R})$, and (b) the cosine of the opening angle between the muon and total proton momentum vector, $\cos(\theta_{\vec{P}_\mu \cdot \vec{P}_{sum}})$. The inner error bands on the data represent the statistical uncertainty while the outer error bands represent the systematic uncertainty. A χ^2/ndf, considering systematic and statistical uncertainties, is calculated between the data and each model set curve. Details of the generator predictions are given in section 3.

When extracting the cross section from data, we find that the GiBUU, GENIE MicroBooNE Tune, and GENIE Nieves models are compatible with our data in $\cos(\theta_{\vec{P}_L \cdot \vec{P}_R})$, and the GiBUU

and NEUT models have the best agreement with our data in $\cos(\theta_{\vec{P}_\mu \cdot \vec{P}_{\mathrm{sum}}})$. The χ^2 per degree of freedom (χ^2/dof) is calculated between the data and each model set curve. The number of degrees of freedom is equal to the number of histogram bins. Both systematic and statistical uncertainties on the data are considered in this calculation.

The GENIE Empirical model over-predicts the normalization in the region of low $\cos(\theta_{\vec{P}_L \cdot \vec{P}_R})$, and has the worst agreement with data as evidenced by the χ^2/dof = 23.91/7. The GENIE SuSAv2 model is over-predicted throughout the reported phase space in both opening-angle distributions which is likely caused by the increased CC2p2h cross-section normalization. Despite the tune of CC2p2h cross-section parameters, the GENIE MicroBooNE and GENIE Nieves predictions have approximately equal agreement with data in both opening angle distributions. The GiBUU model set is found to have the best agreement in both distributions.

We further show the single differential cross sections for the data and the models as functions of δP_T in Fig. 3. In this variable, NuWro has a larger normalization than any other model or data in the first bin which drives the high χ^2/dof = 16.33/6. The reason for this is that Nieves and NuWro form their initial hadronic states in different ways. In the GENIE implementation of the GENIE Nieves model set, two nucleons are selected from the Fermi sea of the nucleus [24]. The momentum of each nucleon is then randomly sampled from a distribution of the initial state nucleon momentum [23] formed from the LFG nuclear model [29]. In NuWro, the selection of the two nucleons and their momenta is similar to the GENIE implementation of GENIE Nieves, but the two nucleons are required to have back-to-back momenta in the initial state [49]. The over-prediction of NuWro at low δP_T has also been observed in Ref. [50], which also finds this over-prediction in the absence of FSI, indicating that the excess is an initial state effect. Our data shows agreement with the NEUT, GiBUU, GENIE Nieves, and GENIE Empirical model sets. The GENIE SuSAv2 model has an over-predicted normalization, whilst the GENIE MicroBooNE tune prediction has a larger disagreement with the data than its base model, GENIE Nieves.

5. Conclusion

In this letter, we present the first measurement of single differential cross sections of CC1μ2p0π events on argon. Events containing exactly one muon, two protons, and no other mesons are selected from BNB data. We extract differential cross sections as functions of three kinematic variables, $\cos(\theta_{\vec{P}_L \cdot \vec{P}_R})$, $\cos(\theta_{\vec{P}_\mu \cdot \vec{P}_{\mathrm{sum}}})$ and δP_T, which are found to be sensitive to the formation of 2p2h pairs through MEC and FSI processes. We compare our extracted cross sections to those predicted by the GENIE, GiBUU, NEUT, and NuWro generators, including four different GENIE model sets. These cross-section models span a range of nuclear models, QE and MEC models, and hadron transport models. We find that the GiBUU prediction shows the best overall shape agreement in the kinematic variables describing opening angles. The δP_T variable is sensitive to the different initial hadronic states, and we find that the NEUT prediction gives the best overall description of the production of CC1μ2p0π final states. This is the first differential cross-section measurement of two-proton final states, and therefore the first time 2p2h/MEC models have been compared to data in an analysis dominated by such interactions. This provides valuable input for future model development toward precision neutrino physics measurements. In addition, these measured CC1μ2p0π cross sections can be used to reinterpret data from existing experiments that cannot distinguish 2p2h final states from other CC interaction mechanisms.
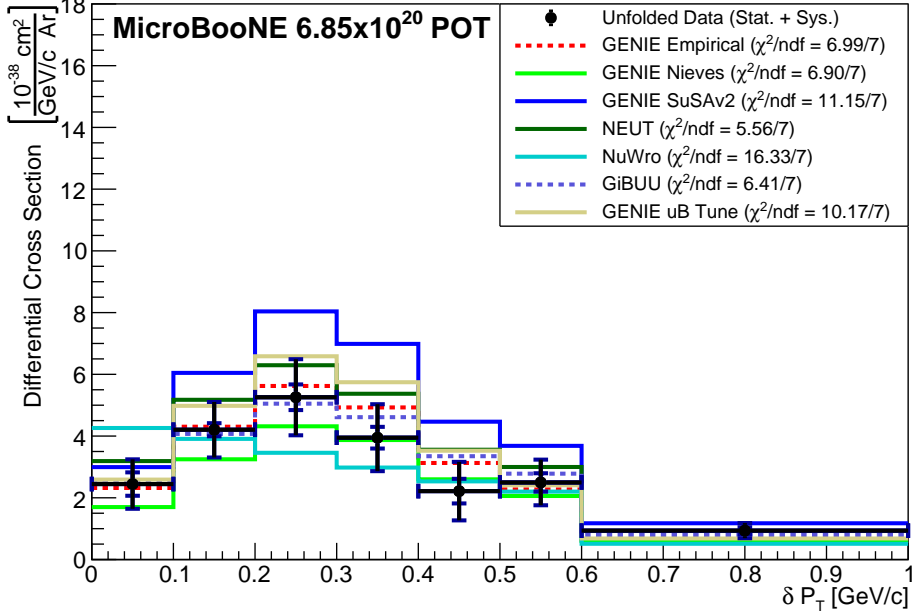
Figure 3: Single differential cross section as a function of the magnitude of the transverse momentum of the final state system, $\delta P_T = \left| \vec{P}_T^{\mu} + \vec{P}_T^{L} + \vec{P}_T^{R} \right|$. The inner error bands on the data represent the statistical uncertainty while the outer error bands represent the systematic uncertainty. A χ^2/ndf, considering systematic and statistical uncertainties, is calculated between the data and each model set curve. Details of the generator predictions are given in section 3.

References

[1] C. Rubbia. The Liquid Argon Time Projection Chamber: A New Concept for Neutrino Detectors. *Report No. CERN-EP-INT-77-08*, CERN-EP-77-08, 5 1977. URL ,http://cds.cern.ch/record/117852/.

[2] H. H. Chen et al. A Neutrino Detector Sensitive to Rare Processes. I. A Study of Neutrino Electron Reactions. *FNAL Proposal 496*, 5 1976. URL https://inspirehep.net/files/df1edf05d33a55edbb411bdebb802f58.

[3] W.J. Willis and V. Radeka. Liquid-argon ionization chambers as total-absorption detectors. *Nucl. Instrum. Meth.*, 120:221–236, 1974. doi: https://doi.org/10.1016/0029-554X(74)90039-1. URL https://www.sciencedirect.com/science/article/pii/0029554X74900391.

[4] D. R. Nygren. The Time Projection Chamber: A New 4π Detector for Charged Particles. *eConf*, C740805:58, 1974. URL https://lss.fnal.gov/conf/C740805/p58.pdf.

[5] J. A. Formaggio and G. P. Zeller. From eV to EeV: Neutrino cross sections across energy scales. *Rev. Mod. Phys.*, 84:1307–1341, 2012. doi: 10.1103/RevModPhys.84.1307. URL https://link.aps.org/doi/10.1103/RevModPhys.84.1307.

[6] L. Alvarez-Ruso et al. (The Neutrino Scattering Theory Experiment Collaboration). Status and challenges of neutrino–nucleus scattering. *Prog. Part. Nucl. Phys.*, 100:1–68, 2018. doi: https://doi.org/10.1016/j.ppnp.2018.01.006. URL https://www.sciencedirect.com/science/article/pii/S0146641018300061.

[7] O. Hen et al. Nucleon-nucleon correlations, short-lived excitations, and the quarks within. *Rev. Mod. Phys.*, 89:045002, 2017. doi: 10.1103/RevModPhys.89.045002. URL https://link.aps.org/doi/10.1103/RevModPhys.89.045002.

[8] R. Cruz-Torres et al. Many-body factorization and position–momentum equivalence of nuclear short-range correlations. *Nature Phys.*, 17:306–310, 2021. doi: 10.1038/s41567-020-01053-7.

[9] I. Ruiz Simo et al. Two-nucleon emission in neutrino and electron scattering from nuclei: The modified convolution approximation. *Ann. Phys.*, 388:323–349, 2018. doi: https://doi.org/10.1016/j.aop.2017.11.029. URL https://www.sciencedirect.com/science/article/pii/S0003491617303512.

[10] S. Dolan, G. D. Megias, and S. Bolognesi. Implementation of the SuSAv2-meson exchange current 1p1h and 2p2h models in GENIE and analysis of nuclear effects in T2K measurements. *Phys. Rev. D*, 101:033003, Feb 2020. doi: 10.1103/PhysRevD.101.033003. URL https://link.aps.org/doi/10.1103/PhysRevD.101.033003.

[11] M. A. Acero et al. (The NOνA Collaboration). Adjusting neutrino interaction models and evaluating uncertainties using NOνA near detector data. *Eur. Phys. J. C*, 80, 2020. doi: 10.1140/epjc/s10052-020-08577-5. URL http://dx.doi.org/10.1140/epjc/s10052-020-08577-5.

[12] P. Abratenko et al. (The MicroBooNE Collaboration). New CC0π GENIE model tune for MicroBooNE. *Phys. Rev. D*, 105:072001, 2022. doi: 10.1103/PhysRevD.105.072001. URL https://link.aps.org/doi/10.1103/PhysRevD.105.072001.

[13] K. Abe et al. (The T2K Collaboration). Measurement of neutrino and antineutrino oscillations by the T2K experiment including a new additional sample of ν_e interactions at the far detector. *Phys. Rev. D*, 96, 2017. doi: 10.1103/physrevd.96.092006. URL http://dx.doi.org/10.1103/PhysRevD.96.092006.

[14] K. Abe et al. (The T2K Collaboration). Measurements of neutrino oscillation parameters from the T2K experiment using 3.6×10^{21} protons on target. *Eur. Phys. J. C*, 83, 2023. doi: 10.1140/epjc/s10052-023-11819-x. URL http://dx.doi.org/10.1140/epjc/s10052-023-11819-x.

[15] R. Acciarri et al. (The ArgoNeuT Collaboration). Detection of back-to-back proton pairs in charged-current neutrino interactions with the ArgoNeuT detector in the NuMI low energy beam line. *Phys. Rev. D*, 90:012008, 2014. doi: 10.1103/PhysRevD.90.012008. URL https://link.aps.org/doi/10.1103/PhysRevD.90.012008.

[16] R. Acciarri et al. (The MicroBooNE Collaboration). Design and construction of the MicroBooNE detector. *J. Instrum.*, 12:P02017–P02017, 2017. doi: 10.1088/1748-0221/12/02/p02017. URL http://dx.doi.org/10.1088/1748-0221/12/02/P02017.

[17] A. A. Aguilar-Arevalo et al. (The MiniBooNE Collaboration). Neutrino flux prediction at MiniBooNE. *Phys. Rev. D*, 79:072002, 2009. doi: 10.1103/PhysRevD.79.072002. URL https://link.aps.org/doi/10.1103/PhysRevD.79.072002.

[18] C. Andreopoulos et al. (The GENIE Collaboration). The GENIE Neutrino Monte Carlo Generator. *Nucl. Instrum. Meth. A*, 614:87–104, 2010. doi: 10.1016/j.nima.2009.12.009. URL https://www.sciencedirect.com/science/article/pii/S0168900209023043.

[19] C. Adams et al. (The MicroBooNE Collaboration). Rejecting cosmic background for exclusive charged current quasi elastic neutrino interaction studies with Liquid Argon TPCs; a case study with the MicroBooNE detector. *Eur. Phys. J. C*, 79:673, 2019. doi: 10.1140/epjc/s10052-019-7184-7. URL https://doi.org/10.1140/epjc/s10052-019-7184-7.

[20] T. Golan, J. T. Sobczyk, and J. Zmuda. NuWro: The Wroclaw Monte Carlo Generator of Neutrino Interactions. *Nucl. Phys. B Proc. Suppl.*, 229-232:499–499, 2012. doi: 10.1016/j.nuclphysbps.2012.09.136.

[21] L. Alvarez-Ruso et al. (The GENIE Collaboration). Recent highlights from GENIE v3. *Eur. Phys. J. ST*, 230:4449–4467, 2021. doi: 10.1140/epjs/s11734-021-00295-7. URL https://doi.org/10.1140/epjs/s11734-021-00295-7.

[22] J. Nieves, J. E. Amaro, and M. Valverde. Inclusive quasielastic charged-current neutrino-nucleus reactions. *Phys. Rev. C*, 70:055503, 2004. doi: 10.1103/PhysRevC.70.055503. URL https://link.aps.org/doi/10.1103/PhysRevC.70.055503.

[23] J. Schwehr, D. Cherdack, and R. Gran. GENIE implementation of IFIC Valencia model for QE-like 2p2h neutrino-nucleus cross section. 2016. URL https://doi.org/10.48550/arXiv.1601.02038.

[24] T. Katori. Meson Exchange Current (MEC) Models in Neutrino Interaction Generators. *AIP Conf. Proc.*, 1663(1): 030001, 2015. doi: 10.1063/1.4919465. URL https://doi.org/10.1063/1.4919465.

[25] R. Acciarri et al. (The MicroBooNE Collaboration). The Pandora multi-algorithm approach to automated pattern recognition of cosmic-ray muon and neutrino events in the MicroBooNE detector. *Eur. Phys. J. C*, 78(1):82, 2018. doi: 10.1140/epjc/s10052-017-5481-6. URL https://doi.org/10.1140/epjc/s10052-017-5481-6.

[26] P. Abratenko et al. (The MicroBooNE Collaboration). Calorimetric classification of track-like signatures in liquid argon TPCs using MicroBooNE data. *J. High Energy Phys.*, 12:153, 2021. doi: 10.1007/J.HighEnergyPhys.12(2021)153. URL https://doi.org/10.1007/JHEP12(2021)153.

[27] R. A. Smith and E. J. Moniz. Neutrino reactions on nuclear targets. *Nucl. Phys. B*, 43:605, 1972. doi: 10.1016/0550-3213(75)90612-4. URL https://doi.org/10.1016/0550-3213(75)90612-4. [Erratum: Nucl. Phys. B 101, 547 (1975)].

[28] C. H. Llewellyn Smith. Neutrino Reactions at Accelerator Energies. *Phys. Rept.*, 3:261–379, 1972. doi: 10.1016/0370-1573(72)90010-5. URL https://doi.org/10.1016/0370-1573(72)90010-5.

[29] J. Nieves, J. E. Amaro, and M. Valverde. Inclusive quasielastic charged-current neutrino-nucleus reactions. *Phys. Rev. C*, 70:055503, 2004. doi: 10.1103/PhysRevC.70.055503. URL https://link.aps.org/doi/10.1103/PhysRevC.70.055503.

[30] J. Nieves et al. Neutrino Energy Reconstruction and the Shape of the CCQE-like Total Cross Section. *Phys. Rev. D*, 85:113008, 2012. doi: 10.1103/PhysRevD.85.113008. URL https://doi.org/10.1103/PhysRevD.85.113008.

[31] B. D. Serot and J. D. Walecka. *Relativistic Nuclear Many-Body Theory*, pages 49–92. Springer US, Boston, MA, 1992. ISBN 978-1-4615-3466-2. doi: 10.1007/978-1-4615-3466-2_5. URL https://doi.org/10.1007/978-1-4615-3466-2_5.

[32] J. A. Caballero et al. Superscaling in charged current neutrino quasielastic scattering in the relativistic impulse approximation. *Phys. Rev. Lett.*, 95:252502, 2005. doi: 10.1103/PhysRevLett.95.252502. URL https://link.aps.org/doi/10.1103/PhysRevLett.95.252502.

[33] T. W. Donnelly and I. Sick. Superscaling in inclusive electron - nucleus scattering. *Phys. Rev. Lett.*, 82:3212–3215, 1999. doi: 10.1103/PhysRevLett.82.3212. URL https://doi.org/10.1103/PhysRevLett.82.3212.

[34] U. Mosel and K. Gallmeister. Lepton-induced reactions on nuclei in a wide kinematical regime. *Phys. Rev. D*, 109, 2024. doi: 10.1103/physrevd.109.033008. URL http://dx.doi.org/10.1103/PhysRevD.109.033008.

[35] T. Golan, J.T. Sobczyk, and J. Żmuda. NuWro: the Wrocław Monte Carlo generator of neutrino interactions. *Nucl. Phys. B Proc. Suppl.*, 229–232:499, 2012. doi: 10.1016/j.nuclphysbps.2012.09.136. URL http://dx.doi.org/10.1016/j.nuclphysbps.2012.09.136.

[36] Y. Hayato and L. Pickering. The NEUT neutrino interaction simulation program library. *Eur. Phys. J. ST*, 230:4469–4481, 2021. doi: 10.1140/epjs/s11734-021-00287-7. URL http://dx.doi.org/10.1140/epjs/s11734-021-00287-7.

[37] T. Leitner, L. Alvarez-Ruso, and U. Mosel. Charged current neutrino-nucleus interactions at intermediate energies. *Phys. Rev. C*, 73, 2006. doi: 10.1103/physrevc.73.065502. URL http://dx.doi.org/10.1103/PhysRevC.73.065502.

[38] U. Mosel. Neutrino event generators: foundation, status and future. *J. Phys. G*, 46:113001, 2019. doi: 10.1088/1361-6471/ab3830. URL http://dx.doi.org/10.1088/1361-6471/ab3830.

[39] R.C. Carrasco and E. Oset. Interaction of real photons with nuclei from 100 to 500 MeV. *Nucl. Phys. A*, 536(3–4): 445–508, 1992. doi: 10.1016/0375-9474(92)90109-w. URL http://dx.doi.org/10.1016/0375-9474(92)90109-W.

[40] J. Nieves, I. Ruiz Simo, and M. J. Vicente Vacas. Inclusive charged-current neutrino-nucleus reactions. *Phys. Rev. C*, 83, 2011. doi: 10.1103/physrevc.83.045501. URL http://dx.doi.org/10.1103/PhysRevC.83.045501.

[41] T. Sjöstrand, S. Mrenna, and P. Skands. Pythia 6.4 physics and manual. *J. High Energy Phys.*, 2006:026–026, 2006. doi: 10.1088/1126-6708/2006/05/026. URL http://dx.doi.org/10.1088/1126-6708/2006/05/026.

[42] X. G. Lu et al. Measurement of nuclear effects in neutrino interactions with minimal dependence on neutrino energy. *Phys. Rev. C*, 94:015503, 2016. doi: 10.1103/PhysRevC.94.015503. URL https://doi.org/10.1103/PhysRevC.94.015503.

[43] A. A. Aguilar-Arevalo et al. (The MiniBooNE Collaboration). First measurement of the muon antineutrino double-differential charged-current quasielastic cross section. *Phys. Rev. D*, 88:032001, 2013. doi: 10.1103/PhysRevD.88.032001. URL https://doi.org/10.1103/PhysRevD.88.032001.

[44] J. Calcutt et al. Geant4Reweight: a framework for evaluating and propagating hadronic interaction uncertainties in Geant4. *J. Instrum.*, 16:P08042, 2021. doi: 10.1088/1748-0221/16/08/P08042. URL url={https://dx.doi.org/10.

1088/1748-0221/16/08/P08042}.

[45] P. Abratenko et al. (The MicroBooNE Collaboration). Novel approach for evaluating detector-related uncertainties in a LArTPC using MicroBooNE data. *Eur. Phys. J. C*, 82:454, 2022. doi: 10.1140/epjc/s10052-022-10270-8. URL https://doi.org/10.1140/epjc/s10052-022-10270-8.

[46] P. Abratenko et al. (The MicroBooNE Collaboration). Search for an anomalous excess of inclusive charged-current ν_e interactions in the MicroBooNE experiment using Wire-Cell reconstruction. *Phys. Rev. D*, 105:112005, 2022. doi: 10.1103/PhysRevD.105.112005. URL https://doi.org/10.1103/PhysRevD.105.112005.

[47] W. Tang et al. Data Unfolding with Wiener-SVD Method. *J. Instrum*, 12:P10002, 2017. doi: 10.1088/1748-0221/12/10/P10002. URL https://doi.org/10.1088/1748-0221/12/10/P10002.

[48] S. Gardiner. Mathematical methods for neutrino cross-section extraction. 2024. doi: 10.48550/arXiv.2401.04065. URL https://arxiv.org/abs/2401.04065.

[49] K. Niewczas and J. T. Sobczyk. Search for nucleon-nucleon correlations in neutrino-argon scattering. *Phys. Rev. C*, 93:035502, 2016. doi: 10.1103/PhysRevC.93.035502. URL https://doi.org/10.1103/PhysRevC.93.035502.

[50] L. Bathe-Peters. Studies of Single-Transverse Kinematic Variables for Neutrino Interactions on Argon. Master's thesis, Berlin Tech U., Harvard U., 2020. URL https://lss.fnal.gov/archive/masters/fermilab-masters-2020-03.pdf.